ECS Journal of Solid State
Science and Technology

OPEN ACCESS

Effect of Electron Injection on Minority Carrier Transport in 10 MeV Proton Irradiated β-Ga_2O_3 Schottky Rectifiers

To cite this article: Sushrut Modak *et al* 2020 *ECS J. Solid State Sci. Technol.* **9** 045018

View the article online for updates and enhancements.

This content was downloaded from IP address 128.227.130.219 on 13/10/2020 at 01:55

ECS Journal of Solid State Science and Technology, 2020 **9** 045018

Effect of Electron Injection on Minority Carrier Transport in 10 MeV Proton Irradiated β-Ga_2O_3 Schottky Rectifiers

Sushrut Modak,[1] Leonid Chernyak,[2,z] Sergey Khodorov,[2] Igor Lubomirsky,[2,*] Arie Ruzin,[3] Minghan Xian,[4] Fan Ren,[4,] and Stephen J. Pearton[5,**]**

[1]*Department of Physics, University of Central Florida, Orlando, Florida 32816, United States of America*
[2]*Department of Materials and Interfaces, Weizmann Institute of Science, Rehovot 76100, Israel*
[3]*Department of Electrical Engineering, Tel Aviv University, Tel Aviv 69978, Israel*
[4]*Department of Chemical Engineering, University of Florida, Gainesville, Florida 32611, United States of America*
[5]*Material Science and Engineering, University of Florida, Gainesville, Florida 32611, United States of America*

We report the effect of extended duration electron beam exposure on the minority carrier transport properties of 10 MeV proton irradiated (fluence $\sim 10^{14}$ cm^{-2}) Si-doped β-Ga_2O_3 Schottky rectifiers. The diffusion length (L) of minority carriers is found to decrease with temperature from 330 nm at 21 °C to 289 nm at 120 °C, with an activation energy of ~26 meV. This energy corresponds to the presence of shallow Si trap-levels. Extended duration electron beam exposure enhances L from 330 nm to 726 nm at room temperature. The rate of increase for L is lower with increased temperature, with an activation energy of 43 meV. Finally, a brief comparison of the effect of electron injection on proton irradiated, alpha-particle irradiated and a reference Si-doped β-Ga_2O_3 Schottky rectifiers is presented.
© 2020 The Author(s). Published on behalf of The Electrochemical Society by IOP Publishing Limited. This is an open access article distributed under the terms of the Creative Commons Attribution Non-Commercial No Derivatives 4.0 License (CC BY-NC-ND, http://creativecommons.org/licenses/by-nc-nd/4.0/), which permits non-commercial reuse, distribution, and reproduction in any medium, provided the original work is not changed in any way and is properly cited. For permission for commercial reuse, please email: oa@electrochem.org. [DOI: 10.1149/2162-8777/ab902b]

Manuscript submitted March 2, 2020; revised manuscript received April 26, 2020. Published May 13, 2020. *This paper is part of the JSS Focus Issue on Gallium Oxide Based Materials and Devices II.*

Gallium oxide is a transparent conductive oxide with an ultra-wide bandgap of ~4.9 eV for the monoclinic β-polymorph. It is a promising material with applications in high-power electronics, true solar-blind photodetectors and sensors.[1–9] The high breakdown field of 8 MV cm^{-1} and electron saturation velocity of 2×10^7 cm s^{-1} produce advantages over GaN and SiC in these applications. Advances in growth techniques have led to β-Ga_2O_3 being available in both bulk single crystal wafer form and high purity epitaxial films with thickness up to tens of microns.[1,5,7,9] With availability of n-type doping with Si and Sn, devices such as Schottky rectifiers, field effect transistors and MOSFETS have been demonstrated.[10–13] P-type doping is a challenge to obtain in most wide bandgap semiconductors, but recently p-type conductivity has been shown to exist under limited conditions in Ga_2O_3.[14] However, it is only available in very low doping levels and hole mobilities, therefore, bipolar technology in Ga_2O_3 without the use of other p-type oxides is yet to flourish.

The bond strength of a semiconductor is correlated to its bandgap.[2,15–23] This property makes gallium oxide intrinsically radiation hard as it takes radiation with a large amount of energy to produce defects in the material. As a result, the applicability of gallium oxide in extreme environments such as high/low temperatures and exposure to hazardous radiation in lower earth satellite orbitals becomes viable.[1] Numerous studies have already been performed to test the radiation hardness of gallium oxide. Exposure to high intensity gamma-ray radiation 230 kGy(SiO_2) of Ga_2O_3 MOSFETS causes degradation in gate oxide with virtually negligible hysteresis in the transfer characteristics.[24] A new trap level with unknown origin at $E_c - 1.29$ eV is introduced and the concentration of existing $E_c - 2.0$ eV increased after exposing Ga_2O_3 to neutron irradiation.[25] In addition, Ga_2O_3 has been successfully shown to detect fast neutrons (14 MeV).[26] Exposure to varying doses of electron radiation (1.5 MeV) produces a carrier removal rate of 4.9 cm^{-1} and two orders of magnitude increase in the on-state resistance of rectifiers at the highest fluence.[27] Moreover, it also deteriorated the radiative recombination lifetime and the diffusion length of minority carriers in the material.[28] Minority carrier transport is of vital importance in electronics and can severely impact the device operation in the event of degradation to its constituent properties such as diffusion length and lifetime. Despite the high radiation hardness of Ga_2O_3 it is still susceptible to degradation to some extent making it unsuitable for applications in hazardous environments for long periods of time. A recent study has shown that when 18 MeV alpha-particle degraded Si-doped β-Ga_2O_3 is exposed to low energy electron beam for extended duration, restores and even enhances the diffusion length.[29] Time-resolved cathodoluminescence measurements on electron injection in GaN have provided a direct evidence in the increase of minority carrier lifetime.[30] So, electron injection has been proved to enhance and mitigate the radiation damage to the two most important characteristics of minority carrier transport, namely diffusion length and lifetime.[30–33] In this study we study the deterioration caused to Si-doped β-Ga_2O_3 Schottky rectifiers due to 10 MeV proton irradiation and mitigation of the radiation incurred damage using the electron injection effect. Solar particle events, that occur at a rate of 1–2 per solar cycle, consist primarily of protons (with energy >10 meV, fluences $>10^{10}$ cm^{-2}).[34,35] Therefore, it is one of the primary sources of material degradation in lower earth satellite orbits and an important phenomenon to apply and study the effect of electron injection. Furthermore, the results are compared to previously reported 18 MeV alpha-particle damage in a similar structure.

Experimental

The Schottky rectifiers used in this study are fabricated on Sn-doped 650 μm thick single crystal β-Ga_2O_3 wafer (001 orientation) grown by edge-defined film-fed growth technique. Si-doped epilayer (~20 μm) was grown with halide vapor phase epitaxy and subsequently thinned down to 10 μm with electromechanical polishing for planarization. The electrically active Sn concentration in the substrate was found to be $\sim 2.2 \times 10^{18}$ cm^{-3} by Hall measurement. Concentration of Si dopants in the epilayer is $\sim 3 \times 10^{16}$ cm^{-3}. Top Schottky contacts and bottom Ohmic contacts were formed by electron beam deposition of Ni/Au (20 nm/80 nm) and Ti/Au (20 nm/80 nm) respectively. Proton irradiation was performed by a 10 MeV proton beam generated by a MC-50 cyclotron at Korea Institute of Radiological and Medical Science with a beam fluence of

*Electrochemical Society Member.
**Electrochemical Society Fellow.
zE-mail: Leonid.Chernyak@ucf.edu

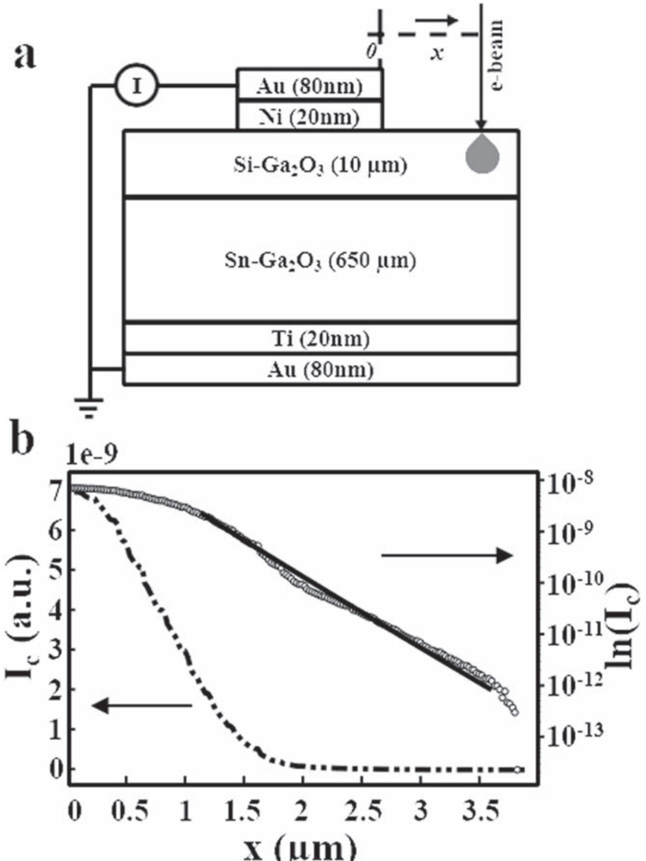

Figure 1. (a) Schematic of the Si-doped β-Ga_2O_3 Schottky rectifiers used in this study. EBIC line-scan is performed by scanning the electron beam laterally across the Schottky barrier. (b) EBIC line-scan raw data (left) and *ln(I)* vs *x* fitted with exp$(-x/L)/x^{\alpha}$ to extract *L* (right).

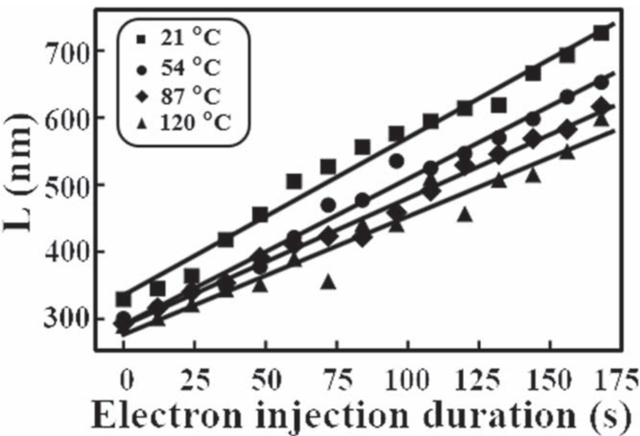

Figure 2. Diffusion length as a function of duration of electron injection for 21 °C, 54 °C, 87 °C and 120 °C. *L* increases linearly with the duration and the rate of increase of *L* decreases with rise in temperature.

10^{14} cm^{-2}. The range of protons in the material was found to be 330 μm, completely irradiating the epilayer and a large portion of the substrate. More details on the fabrication process can be found elsewhere.[36] Figure 1a shows a schematic diagram showing the structure of the Schottky rectifiers used in this study.

Electron Beam-Induced Current (EBIC) line-scan technique is used to measure the diffusion length of minority carriers (*L*) with the help of Phillips XL-30 Scanning Electron Microscope (SEM). The temperature control is achieved from room to 120 °C with Gatan MonoCL2 temperature-controlled stage with 0.5 °C accuracy integrated into the SEM. Planar-mode configuration of EBIC line-scan with metal-semiconductor Schottky contact is employed to measure *L*. For all measurements, beam energy is kept fixed at 10 keV (absorbed current ~0.4 nA), which gives a maximum electron range (R_e) of 0.715 μm in the material with Kanaya-Okayama method.[37]

As will be seen in the following section, this ensures the ratio $R_e/L < 4$ making sure that the diffusion length is not EBIC resolution limited.[38] Moreover, the sample thickness (*h*) is much larger than the R_e, ensuring that it does not limit collection of the generated carriers. The EBIC line-scan technique is depicted in Fig. 1a, the electron beam is scanned across the edge of the Schottky contact moving radially outwards. Each line-scan took ~6 s scanning a total distance of ~4.8 μm. As the beam is scanned, non-equilibrium electron-hole pairs are generated at the point of impact and diffuse outwards. The carrier pairs that are swept towards the space-charge region near the Schottky contact are separated and only the minority carriers (holes, in this case) are collected by the contact. The current, induced due to non-equilibrium minority carriers, is amplified with Stanford Research Systems Low-Noise Amplifier (SR570) and then recorded with Keithley DMM 2000 digital multimeter connected to a PC with LabView interface. Electron injection was performed by continuously repeating the EBIC line-scan at the same location for extended duration (up to 175 s). EBIC signal was recorded at the same time to see the evolution of diffusion length (*L*) in the affected area as a function of duration of electron bombardment. Every instance of electron injection is performed at a new location due to the sensitivity of the material to this effect.

Results and Discussion

Diffusion length is the total distance carriers travel before undergoing recombination. It can be obtained from EBIC line-scan by fitting the acquired signal to the following empirical relation[39–42]

$$I_c(x) = I_0 x^{\alpha} \exp\left(-\frac{x}{L}\right), \quad [1]$$

where, I_c is the measured EBIC signal, I_0 is s scaling constant, *x* is distance from the semiconductor-metal junction, *L* is the diffusion length of minority holes and α is a constant related to surface recombination velocity. It was noticed that $x > 2L$ for every line-scan, ensuring the accuracy of extracted *L* values.[43] For this analysis, α is kept constant at -1.5 as it results in the best fit for EBIC line-scan data. Figure 1b shows an example of a line-scan. Axis on left shows the raw EBIC signal and on right, *ln(I)* vs *x* is fitted with exp$(-x/L)/x^{\alpha}$. Line-scans are continuously repeated to induce electron injection effect at every temperature. EBIC signal is simultaneously recorded to extract *L* and determine its evolution as a function of electron injection duration.

Figure 2 shows a plot of *L* as a function of duration of electron injection at temperatures from room to 120 °C. It is observed that *L* linearly increases with time, from 330 nm up to 726 nm in 175 s. At higher temperatures, the rate of *L* increase goes down. At 120 °C, *L* increases from 289 nm to 598 nm in the same duration. The temperature dependent activation energy for the electron injection effect can be obtained by[44]

$$R(T) = R_0 \exp\left(\frac{\Delta E_{A,T}}{2kT}\right) \exp\left(\frac{\Delta E_{A,I}}{kT}\right), \quad [2]$$

where, *R* is the slope of *L* increase with duration of electron injection (from Fig. 2), R_0 is a scaling constant, $\Delta E_{A,T}$ is thermal activation energy, $\Delta E_{A,I}$ is the activation energy for temperature dependence of electron injection effect, *k* is the Boltzmann constant, and *T* is the temperature. Figure 3a shows a plot of *R* as a function of temperature. The increase in *L* is attributed to carrier trapping or electron injection effect. Due to extended duration of electron beam

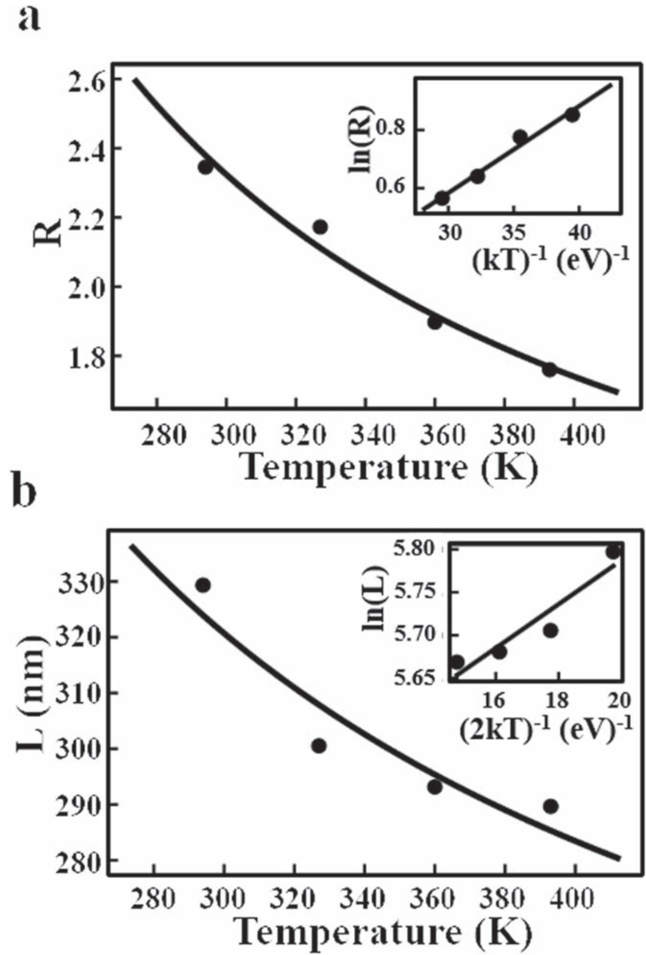

Figure 3. (a) Plot depicting the rate for increase of L with temperature fitted with Eq. 2. $\Delta E_{A,I}$ is calculated from the Arrhenius plot in the inset, if $\Delta E_{A,T}$ is known. $\Delta E_{A,T}$ is obtained from the temperature dependence of L, which is obtained from a single line-scan, virtually without a trace of electron injection effect (see (b) below).(b) Temperature dependence of L and fitted with Eq. 3. $\Delta E_{A,T}$ is calculated from the Arrhenius plot in the inset.

bombardment, excess non-equilibrium electrons are generated in the material. These electrons occupy the trap states responsible for carrier recombination. With longer electron beam exposure, the number of trapped electrons continues to rise, making these states unavailable in the recombination process.[29,31,44] The rise in the non-equilibrium carrier lifetime (τ) directly affects L as $L = \sqrt{D\tau}$, where D is the diffusion coefficient in the material. The increase in L was attributed to the rise in τ as mobility ($\sim D$) was assumed to be constant. This effect has been validated in a comprehensive study of electron injection effect in GaN. Experimental evidence of increase in L due to electron injection was found to be directly correlated to the increase in $\sqrt{\tau}$.[30,45] Moreover, in a different study, Ga_2O_3 Schottky rectifiers were irradiated with high energy electrons (1.5 MeV), and both L and τ showed a monotonic reduction with the increase in the electron fluence.[28] This suggests a similar mechanism at play in the current structure. Furthermore, a similar increase in L with electron injection effect was observed in ZnO. Firstly, L was saturated with electron injection effect at room temperature to ~2.25 μm. Upon thermal annealing at 175 °C over a duration of 30 min, a pronounced decrease of 1 μm was seen in L. This effect further reinforces the involvement of electron traps in the recombination process. Thermal activation of the trapped carriers restores the original recombination pathways, resulting in reduced L. Moreover, the increase in L was observed to last for several days. Similar trend was observed in the case of Ga_2O_3 in this study, but a complete comparison of the decay rates of electron injection enhanced L in reference, alpha-particle irradiated and proton irradiated structures will be addressed in a follow-up study.

Table I. A comparison of the L, $\Delta E_{A,T}$ & $\Delta E_{A,I}$ for the reference, 10 MeV proton irradiated and 18 MeV alpha-particle irradiated Si-doped β-Ga_2O_3 Schottky rectifiers.

Parameter	Reference	18 MeV Alpha-particle	10 MeV Proton
L (nm)	427	378	330
$\Delta E_{A,T}$ (meV)	53	29	26
$\Delta E_{A,I}$ (meV)	74	49	43

From Figs. 2 and 3a, the rate of increase of L clearly decreases with rise in temperature. If $\Delta E_{A,T}$ is known, $\Delta E_{A,I}$ can be calculated from the slope of the Arrhenius plot in the inset of Fig. 3a. $\Delta E_{A,T}$ can be obtained by studying the variation of L with temperature without or "zero" electron injection as shown in Fig. 3b. These are single line-scans acquired at the respective temperature with virtually no contribution of electron injection effect. The temperature dependence of L can be written as.[44,46]

$$L(T) = L_0 \exp\left(\frac{\Delta E_{A,T}}{2kT}\right), \quad [3]$$

where, L_0 is a scaling constant. $\Delta E_{A,T}$ is obtained as ~26 meV from the slope of the Arrhenius plot in the inset of Fig. 3b. Independent studies have attributed this activation energy to shallow trap levels formed by Si donors.[47,48] Moreover, L decreases from 330 nm to 289 nm with rise in temperature from 21 °C to 120 °C. This temperature dependence of L and the associated thermal activation energy closely matches the previously reported results on a similar structure.[36] The reduction in L could occur either from the temperature dependence of carrier recombination lifetime or enhanced scattering due to carrier-phonon interaction at high temperatures.[49,50] For identification of the dominating factor, temperature dependent lifetime measurements, which are currently instrument limited and will be addressed in future studies. Knowing $\Delta E_{A,T}$, $\Delta E_{A,I}$ is obtained as ~43 meV.[44] Previous work on similar unirradiated Si-doped β-Ga_2O_3 Schottky rectifier found out the value of $\Delta E_{A,I}$ to be 74 meV,[29] corresponding to a yet unknown trap state.[51] It was found that radiation damage introduces additional trap states and recombination centers in the bandgap. The existence of these trap states is responsible for a lower rate of L rise with duration of electron injection.

10 MeV protons and 18 MeV alpha-particles are known to produce point defects in Ga_2O_3.[52,53] It was shown that protons create a wide range of trap states and defects spanning the entire bandgap, a dominant defect a being shallow Hydrogen donor level.[54] It was observed that 10 MeV protons with fluence ~10^{14} cm^{-2} produce a carrier removal rate of ~235 cm^{-1}. On the other hand, alpha-particles primarily produce a large number of vacancies in clusters at the end of their trajectory.[53] In Ga_2O_3, they have a carrier removal rate of 406–728 cm^{-1} for fluences of 10^{12}–10^{13}cm^{-2}. Furthermore, radiation damage can also increase the density of native trap levels.[53,54] A comparison of results from the proton irradiated structure in this study, previously reported alpha-particle irradiated (18 MeV fluences of $10^{12}-10^{13}$ cm^{-2}) and reference Si-doped β-Ga_2O_3 Schottky rectifiers is shown in Table I. The room temperature L for reference structure is largest at 427 nm and reduces to 378 nm and 330 nm for alpha-particle and proton irradiated structures, respectively. Furthermore, difference in $\Delta E_{A,T}$ for reference and proton irradiated structure is ~27 meV and ~31 meV for $\Delta E_{A,I}$. These values are comparable and indicate towards a common underlying deterioration effect due to radiation damage. For alpha-particle irradiated sample, the energy differences compared to reference structure are ~24 meV and ~25 meV respectively, reinforcing the previous assertion.

To summarize, the incident low energy electron beam creates non-equilibrium carrier pairs in the material and just the minority carriers (holes, in this case) are recorded through EBIC measurement. Trap-states in the bandgap, which provide a recombination pathway, are occupied by the excess non-equilibrium electrons due to prolonged exposure to the electron beam. This, in turn, causes reduction in the recombination rate and is responsible for prolongation of L. Radiation damage creates additional defects in the material which compounds the recombination process and reduces L. Moreover, prolonged exposure of the irradiated structure to electron beam causes trap saturation, but since the number of traps is larger than in the reference structure, the rate at which L increases, is comparatively lower. Temperature plays an important role in electron injection and the raw value of L. The base value of L and the rate at which it increases with temperature, monotonically reduces for higher temperatures. Additionally, temperature measurements enable the determination of activation energies, namely $\Delta E_{A,T}$ & $\Delta E_{A,I}$, which were calculated for both proton and alpha-particle irradiated structures as discussed above. The consistency in the measured minority carrier transport properties due to the 10 MeV proton irradiation damage and 18 MeV alpha-particle damage validate that the same underlying mechanism is responsible in this case.

Conclusions

In conclusion, the diffusion length (L) of holes in Si-doped β-Ga_2O_3 Schottky rectifiers was measured at temperatures ranging from room to 120 °C. L decreases from 330 nm at room temperature to 289 nm at 120 °C. The temperature dependent activation energy for change in L was found to be 26 meV and is attributed to shallow Si trap levels. The activation energy for temperature dependence of electron injection effect was calculated as 43 meV. Finally, the effect of proton irradiation was compared to alpha-particle irradiation and a control reference structure. The effect of electron injection in both types of radiation damage was found to be similar in nature with comparable activation energies for temperature dependence of L and the electron injection effect.

Acknowledgments

Research at UCF and the Weizmann institute was supported in part by North Atlantic Treaty Organization (NATO) (award # G5453) and National Science Foundation, Division of Materials Research (NSF) (UCF award # ECCS1802208). Research at UCF and Tel Aviv University was supported in part by United States-Israel Binational Science Foundation (US-Israel BSF) (2018010). The work at UF was sponsored by the Department of Defense, Defense Threat Reduction Agency, HDTRA1-17-1-011, monitored by Jacob Calkins and also by National Science Foundation, Division of Materials Research (NSF DMR) 1856662 (Tania Paskova).

ORCID

Sushrut Modak https://orcid.org/0000-0003-0752-5662
Stephen J. Pearton https://orcid.org/0000-0001-6498-1256

References

1. S. J. Pearton, J. Yang, P. H. Cary, F. Ren, J. Kim, M. J. Tadjer, and M. A. Mastro, *Appl. Phys. Rev.*, **5**, 011301 (2018).
2. J. Y. Tsao et al., *Adv. Electron. Mater.*, **4**, 1600501 (2018).
3. M. Higashiwaki and G. H. Jessen, *Appl. Phys. Lett.*, **112**, 060401 (2018).
4. H. von Wenckstern, *Adv. Electron. Mater.*, **3**, 1600350 (2017).
5. M. A. Mastro, A. Kuramata, J. Calkins, J. Kim, F. Ren, and S. J. Pearton, *ECS J. Solid State Sci. Technol.*, **6**, P356 (2017).
6. M. Kim, J.-H. Seo, U. Singisetti, and Z. Ma, *Journal of Materials Chemistry C*, **5**, 8338 (2017).
7. S. I. Stepanov, V. I. Nikolaev, V. E. Bougrov, and A. E. Romanov, *Review of Advanced Material Science*, **44**, 63 (2016).
8. M. Higashiwaki, K. Sasaki, H. Murakami, Y. Kumagai, A. Koukitu, A. Kuramata, T. Masui, and S. Yamakoshi, *Semicond. Sci. Technol.*, **31**, 11 (2016).
9. K. Akito, K. Kimiyoshi, W. Shinya, Y. Yu, M. Takekazu, and Y. Shigenobu, *Jpn. J. Appl. Phys.*, **55**, 1202A1202 (2016).
10. M. H. Wong, K. Sasaki, A. Kuramata, S. Yamakoshi, and M. Higashiwaki, *IEEE Electron Device Lett.*, **37**, 212 (2016).
11. M. J. Tadjer, N. A. Mahadik, V. D. Wheeler, E. R. Glaser, L. Ruppalt, A. D. Koehler, K. D. Hobart, C. R. Eddy, and F. J. Kub, *ECS J. Solid State Sci. Technol.*, **5**, P468 (2016).
12. A. J. Green et al., *IEEE Electron Device Lett.*, **37**, 902 (2016).
13. K. D. Chabak et al., *Appl. Phys. Lett.*, **109**, 213501 (2016).
14. E. Chikoidze et al., *Mater. Today Phys.*, **3**, 118 (2017).
15. V. D. Wheeler, D. I. Shahin, M. J. Tadjer, and C. R. Eddy, *ECS J. Solid State Sci. Technol.*, **6**, Q3052 (2016).
16. J. Nord, K. Nordlund, and J. Keinonen, *Phys. Rev. B*, **68**, 184104 (2003).
17. S. J. Pearton, Y. S. Hwang, and F. Ren, *JOM*, **67**, 1601 (2015).
18. A. P. Karmarkar, B. D. White, D. Buttari, D. M. Fleetwood, R. D. Schrimpf, R. A. Weller, L. J. Brillson, and U. K. Mishra, *IEEE Trans. Nucl. Sci.*, **52**, 2239 (2005).
19. J. R. Srour and J. W. Palko, *IEEE Trans. Nucl. Sci.*, **53**, 3610 (2006).
20. S. J. Pearton, R. Deist, F. Ren, L. Liu, A. Y. Polyakov, and J. Kim, *Journal of Vacuum Science & Technology A: Vacuum, Surfaces, and Films*, **31**, 16 (2013).
21. A. Y. Polyakov, S. J. Pearton, P. Frenzer, F. Ren, L. Liu, and J. Kim, *J. Mater. Chem. C*, **1**, 877 (2013).
22. J. D. Greenlee, P. Specht, T. J. Anderson, A. D. Koehler, B. D. Weaver, M. Luysberg, O. D. Dubon, F. J. Kub, T. R. Weatherford, and K. D. Hobart, *Appl. Phys. Lett.*, **107**, 083504 (2015).
23. E. E. Patrick, M. Choudhury, F. Ren, S. J. Pearton, and M. E. Law, *ECS J. Solid State Sci. Technol.*, **4**, Q21 (2015).
24. M. H. Wong, A. Takeyama, T. Makino, T. Ohshima, K. Sasaki, A. Kuramata, S. Yamakoshi, and M. Higashiwaki, *Appl. Phys. Lett.*, **112**, 023503 (2018).
25. E. Farzana, M. F. Chaiken, T. E. Blue, A. R. Arehart, and S. A. Ringel, *APL Mater.*, **7**, 022502 (2019).
26. D. Szalkai, Z. Galazka, K. Irmscher, P. Tutto, A. Klix, and D. Gehre, *IEEE Trans. Nucl. Sci.*, **64**, 1574 (2017).
27. J. Yang, F. Ren, S. J. Pearton, G. Yang, J. Kim, and A. Kuramata, *J. Vac. Sci. Technol. B Nanotechnol. Microelectron.*, **35**, 031208 (2017).
28. J. Lee, E. Flitsiyan, L. Chernyak, J. Yang, F. Ren, S. J. Pearton, B. Meyler, and Y. J. Salzman, *Appl. Phys. Lett.*, **112**, 082104 (2018).
29. S. Modak, L. Chernyak, S. Khodorov, I. Lubomirsky, J. Yang, F. Ren, and S. J. Pearton, *ECS J. Solid State Sci. Technol.*, **8**, Q3050 (2019).
30. S. Modak, L. Chernyak, I. Lubomirsky, and S. Khodorov, *NATO SPS Cluster Workshop on Advanced Technologies* (In Press. Springer), Leuven, Belgium (2019).
31. S. Modak, J. Lee, L. Chernyak, J. Yang, F. Ren, S. J. Pearton, S. Khodorov, and I. Lubomirsky, *AIP Adv.*, **9**, 015127 (2019).
32. L. Chernyak, G. Nootz, and A. Osinsky, *Electron. Lett*, **37**, 922 (2001).
33. L. Chernyak, A. Osinsky, V. Fuflyigin, and E. F. Schubert, *Appl. Phys. Lett.*, **77**, 875 (2000).
34. E. R. Benton and E. V. Benton, *Nucl. Instrum. Methods Phys. Res. B*, **184**, 255 (2001).
35. M. A. Shea and D. F. Smart, *Sol. Phys.*, **127**, 297 (1990).
36. J. Yang, Z. Chen, F. Ren, S. J. Pearton, G. Yang, J. Kim, J. Lee, E. Flitsiyan, L. Chernyak, and A. Kuramata, *Journal of Vacuum Science & Technology B, Nanotechnology and Microelectronics: Materials, Processing, Measurement, and Phenomena*, **36**, 011206 (2018).
37. K. Kanaya and S. Okayama, *J. Phys. D: Appl. Phys.*, **5**, 43 (1972).
38. K. L. Luke, O. von Roos, and L. J. Cheng, *J. Appl. Phys.*, **57**, 1978 (1985).
39. H. J. Leamy, *J. Appl. Phys.*, **53**, R51 (1982).
40. D. E. Ioannou and C. A. Dimitriadis, *Ieee T Electron Dev*, **29**, 445 (1982).
41. C. A. Dimitriadis, *J. Phys. D: Appl. Phys.*, **14**, 2269 (1981).
42. F. Berz and H. K. Kuiken, *Solid-State Electronics*, **19**, 437 (1976).
43. D. S. H. Chan, V. K. S. Ong, and J. C. H. Phang, *IEEE T. Electron Dev.*, **42**, 963 (1995).
44. O. Lopatiuk-Tirpak et al., *J. Appl. Phys.*, **100**, 086101 (2006).
45. S. Modak, L. Chernyak, I. Lubomirsky, S. Khodorov, M. Xian, F. Ren, and S. J. Pearton (Manuscript under preparation).
46. M. Eckstein and H. U. Habermeier, *J. Phys. IV*, **01**, C6-23-C6-28 (1991).
47. H. Masataka, K. Akito, M. Hisashi, and K. Yoshinao, *J. Phys. D: Appl. Phys.*, **50**, 333002 (2017).
48. A. T. Neal et al., *Appl. Phys. Lett.*, **113**, 062101 (2018).
49. T. Onuma, S. Saito, K. Sasaki, K. Goto, T. Masui, T. Yamaguchi, T. Honda, A. Kuramata, and M. Higashiwaki, *Appl. Phys. Lett.*, **108**, 101904 (2016).
50. N. Ma, N. Tanen, A. Verma, Z. Guo, T. Luo, H. Xing, and D. Jena, *Appl. Phys. Lett.*, **109**, 212101 (2016).
51. T. T. Huynh, L. L. C. Lem, A. Kuramata, M. R. Phillips, and C. Ton-That, *Phys. Rev. Mater.*, **2**, 105203 (2018).
52. A. Y. Polyakov, N. B. Smirnov, I. V. Shchemerov, E. B. Yakimov, J. Yang, F. Ren, G. Yang, J. Kim, A. Kuramata, and S. J. Pearton, *Appl. Phys. Lett.*, **112**, 032107 (2018).
53. J. Yang, C. Fares, Y. Guan, F. Ren, S. J. Pearton, J. Bae, J. Kim, and A. Kuramata, *Journal of Vacuum Science & Technology B*, **36**, 031205 (2018).
54. J. Kim, S. J. Pearton, C. Fares, J. Yang, F. Ren, S. Kim, and A. Y. Polyakov, *Journal of Materials Chemistry C*, **7**, 10 (2019).